Charge Density and Bonding in (5,10,15,20-Tetramethylporphyrinato)nickel(II): A Combined Experimental and Theoretical Study†

F. W. Kutzler,[1a] P. N. Swepston,[1b] Ziva Berkovitch-Yellin,[1c] D. E. Ellis,*[1a,b] and James A. Ibers*[1b]

Contribution from the Departments of Physics and Chemistry and the Materials Research Center, Northwestern University, Evanston, Illinois 60201, and the Department of Structural Chemistry, Weizmann Institute of Science, Rehovot, Israel. *Received September 13, 1982*

Abstract: The valence electron distribution in (5,10,15,20-tetramethylporphyrinato)nickel(II), Ni(TMP), has been investigated by experimental and theoretical techniques. An extensive ($(\sin\theta)/\lambda \leq 1.0$ Å^{-1}), low-temperature (140 K) set of crystallographic data has been analyzed by the $(X - X_{HO})$ method in order to extract experimental deformation densities. In addition, model deformation densities have been mapped after a least-squares refinement of deformation functions with the use of a multipole model. First-principles molecular calculations on Ni(TMP), the unsubstituted (porphyrinato)nickel(II), Ni(P), and a model of Ni(TMP) perturbed by neighboring molecules were carried out with the use of the self-consistent local density model. One-electron energy levels, wave functions, and charge densities were obtained from the discrete variational method in an LCAO basis. The experimental and theoretical deformation maps show features qualitatively in agreement. The theoretical effects of the perturbing neighboring molecules show some interesting charge density shifts, but are probably too small to account conclusively for the observed difference in Ni–N bond lengths of 0.020 (1) Å (conventional refinement). A distorted molecule calculation does, however, reproduce essential features of the experimental density distribution.

The importance of metalloporphyrins in biochemistry can hardly be overstated.[2] These versatile prosthetic groups enable reversible binding and transfer of oxygen in heme proteins such as myoglobin and hemoglobin, take part in respiratory electron transport via a sequence of protein and iron porphyrin complexes known as cytochromes, and are part of several enzymes that mediate cellular oxidation–reduction reactions. Furthermore, the process of photosynthesis is founded on the chlorophylls, reduced porphyrins that contain Mg. An understanding on a quantum mechanical basis of why metalloporphyrins play such an important and varied role in biological systems is a significant challenge to modern calculational chemistry.

In this paper we describe a combined experimental and theoretical study of the charge density in the metalloporphyrin Ni(TMP).[3] In addition to being a model for the metalloporphyrins of biological significance, Ni(TMP) is electronically and structurally a very interesting molecule in its own right. It forms a π-molecular compound with the organic acceptor molecule 7,7,8,8-tetracyanoquinodimethane, TCNQ.[4] The reaction of Ni(TMP) and I_2 affords the highly conducting compound Ni(TMP)I.[5] In the crystalline state Ni(TMP) is a planar molecule that packs in one-dimensional stacks of overlapping molecules.[6] In the light of interest in π-complexes[7-15] of metalloporphyrins Ni(TMP) is a good system for studying the electronic effects of intermolecular interactions between metalloporphyrins and aromatic molecules. From a practical standpoint Ni(TMP) is an excellent candidate for a combined experimental and theoretical investigation of valence electron distribution. It forms high quality crystals, a condition that is necessary for a high-resolution X-ray crystallographic study. In addition, the methyl side chains are not subject to disorder, as are frequently the ethyl side chains of the octaethylporphyrins,[16] nor are the methyl groups expected to perturb the electronic nature of the porphyrin core to the extent that the phenyl rings in the tetraphenylporphyrins do. Finally, the related complex (5,10,15,20-tetramethylchlorinato)nickel(II) has been prepared[17,18] and studied crystallographically.[6] A combined experimental and theoretical study of the charge density in this chlorin, a reduced porphyrin, is in progress. Ultimately, we will be able to provide detailed comparisons of the charge density in Ni(TMP) and its metallochlorin analogue, Ni(TMC).

In the routine low-temperature crystallographic investigation of *bis*(*tert*-butylisocyanide)(*meso*-tetraphenylporphyrinato)iron(II)–*bis*(toluene), we first demonstrated the feasibility of mapping valence electron density for metalloporphyrins.[19] More recently

Table I. Details on the Refinement of Structural Data for Ni(TMP)[a]

	conventional refinement	high-order refinement	multipole refinement
$\lambda^{-1}\sin\theta$, Å^{-1}	0.0–1.0	0.7–1.0	0.0–1.0
no. of observtns included in refinement	7365	4676	4438
no. of variables	133	133	224[c]
$R(F^2)$	0.073	0.087[b]	0.051
$R_w(F^2)$	0.109	0.125[b]	0.074
$R(F); F_o^2 > 3\sigma(F_o^2)$	0.042	0.045	0.038
scale factor	3.029 (4)	2.974 (3)	3.00 (2)

[a] The conventional and high-order refinements were carried out on F^2 with the use of all measured intensities within the appropriate $\lambda^{-1}\sin\theta$ (Å^{-1}) range. The multipole refinement was carried out on F with reflections for which $F_o^2 > 3\sigma(F_o^2)$. [b] Based on 7365 observations. [c] Symmetries imposed on the deformation parameters: (a) *mmm* symmetry for Ni; (b) *mm*2 symmetry for N(1) and N(2); (c) *m* symmetry for C_a, C_b, and C_m[36] with C(1)=C(4)=C(6)=C(9), C(2)=C(3)=C(7)=C(8), and C(5)=C(10); (d) C_3 symmetry for C_{methyl} atoms with C(11)=C(12).

† Dedicated to Prof. Jack Dunitz on the occasion of his 60th birthday, March 29, 1983.

(1) (a) Department of Physics, Northwestern Univeristy. (b) Department of Chemistry, Northwestern University. (c) The Weizmann Institute.

(2) The broad topics mentioned in the following paragraphs are discussed: (a) "The Porphyrins"; Dolphin, D., Ed.; Academic Press: New York, 1979; Vol. 1–7. (b) Lehninger, A. "Biochemistry", 2nd ed.; Worth: New York, 1975. (c) "Inorganic Biochemistry"; Eichhorn, G. L.; Ed.; Elsevier: Amsterdam, 1973; Vol. 1–2. (d) Stryer, L. "Biochemistry"; W. H. Freeman: San Francisco, CA, 1975.

(3) Abbreviations: TMP = 5,10,15,20-tetramethylporphyrinato; TPP = 5,10,15,20-tetraphenylporphyrinato.

(4) Pace, L. J.; Ulman, A.; Ibers, J. A. *Inorg. Chem.* **1982**, *21*, 199–207.
(5) Pace, L. J.; Martinsen, J.; Ulman, A.; Hoffman, B. M.; Ibers, J. A. *J. Am. Chem. Soc.* **1983**, *105*, 2612.
(6) Gallucci, J. C.; Swepston, P. N.; Ibers, J. A. *Acta Crystallogr., Sect. B.* **1982**, *B38*, 2134–2139.
(7) Fulton, G. P.; La Mar, G. N. *J. Am. Chem. Soc.* **1976**, *98*, 2119–2128.
(8) Kirner, J. F.; Reed, C. A.; Scheidt, W. R. *Ibid.* **1977**, *99*, 1093–1101.
(9) Scheidt, W. R.; Kastner, M. E.; Hatano, K. *Inorg. Chem.* **1978**, *17*, 706–710.
(10) Scheidt, W. R.; Reed, C. A. *Inorg. Chem.* **1978**, *17*, 710–714.
(11) Hill, H. A. O.; MacFarlane, A. J.; Williams, R. J. P. *J. Chem. Soc. A* **1969**, 1704–1707.
(12) Hill, H. A. O.; Sadler, P. J.; Williams, R. J. P.; Barry, C. D. *Ann. N.Y. Acad. Sci.* **1973**, *206*, 247.

0002-7863/83/1505-2996$01.50/0

Stevens has determined the bonding and lone-pair electron density distribution in (*meso*-tetraphenylporphyrinato)cobalt(II) (Co(TPP)) from a high-resolution, low-temperature crystallographic study.[20] Through our theoretical study of the electronic structures of free-base and transition-metal tetraazaporphyrins[21] we showed the applicability of the first-principles local density model to metalloporphyrin systems. Here we combine these experimental and theoretical techniques to describe the valence electron density of Ni(TMP).

Experimental Section

Crystallographic Procedures. A preliminary account[17] of the crystal structure of Ni(TMP) based on a less accurate data set as well as a conventional X-ray analysis[6] of the present data set have appeared. The compound Ni(TMP) crystallizes in space group C_{2h}^5-$P2_1/c$ with two formula units in a cell of dimensions a = 11.332 (3) Å, b = 5.664 (2) Å, c = 14.162 (4) Å, and β = 104.80 (1)°. A crystallographic center of symmetry is imposed on the molecule. Some details on the conventional refinement along with the present refinements are given in Table I.

A deficiency in conventional X-ray crystallographic modeling is the use of spherical atom scattering factors.[22] This is evident at the end of a typical least-squares refinement process when it is not uncommon to see features in a difference electron density map that are attributable to bonding and lone-pair density. The derived positional and thermal parameters can be biased if the aspherical valence electron density of an atom is significantly unsymmetrical. The spherical atom model is more acceptable for use in the refinement of high-angle (θ) data, since the scattering at high angles is primarily from the core electrons. Consequently, a procedure that is effective for extracting aspherical charge density from X-ray data involves the subtraction of high-order (HO) model density from observed density to give *observed* deformation maps, usually denoted $(X - X_{HO})$.[23]

The present high-order refinement was based on the 4676 reflections (including negative observed intensities) in the range $0.7 \leq \lambda^{-1} \sin\theta \leq 1.0$ Å^{-1}. The quantity minimized was $(\sum(F_o^2 - k^2F_c^2)^2)/(\sigma^2(F_o^2))$, where F_o and F_c are the observed and calculated structure factors and where k is the scale factor. Atomic scattering factors and anomalous dispersion terms were those used earlier.[6] Initially, hydrogen atoms were included in fixed, idealized positions (C–H = 0.95 Å). At the end of the refinement process the hydrogen atom positions were recalculated with C–H = 1.09 Å. As expected, there were modestly high correlations between the scale factor k and the principal thermal parameters of Ni (β_{11}, 0.88; β_{22}, 0.86; β_{33}, 0.90). A difference electron density map calculated at this stage showed a charge buildup of 1.87 e/Å^3 centered on the Ni atom. Following current wisdom we reduced this effect by the refinement of only the scale factor, based on the intensities to be used to calculate the observed deformation maps. Another popular approach is to keep the scale factor from the conventional refinement constant during the high-order refinement and then refine it in an additional cycle.[24] Such a treatment of the present data led in the deformation maps to a negative region centered on the Ni atom with virtually no positive deformation density surrounding the metal in the plane of the porphyrin. We opted for the former method because the deformation density around the metal is emphasized, although some detail is lost owing to superposition with the large positive peak. *Observed* deformation maps were calculated from all measured intensities in the range $0.0 \leq \lambda^{-1} \sin\theta \leq 0.7$ Å^{-1} with negative values of F^2 set to zero. The estimated standard deviation in these maps is 0.11 e/Å^3, as derived from the formalism based on ΔF^2.[25]

Another approach to the treatment of aspherical valence electron density is to include refinable deformation parameters in the least-squares model. We used the multipole model[26] developed by Hansen and Coppens[27] that allows local chemical symmetry to be imposed (Table I). Deformations up to the hexadecapole level were included for all nonhydrogen atoms. Hydrogen atoms were included in fixed, idealized positions with C–H = 1.09 Å. Initially the multipole refinement was based on F^2 but convergence was not achieved. Accordingly we followed current wisdom and carried out the refinement on F. The quantity minimized in the least-squares refinement was $(\sum(|F_o| - k|F_c|)^2)/(\sigma^2(F_o))$, where $\sigma(F_o) = 0.5\sigma(F_o^2)/|F_o|$; use was made of the 4438 intensities with $F_o^2 > 3\sigma(F_o^2)$. *Model* deformation maps[20,23,28] were calculated as multipole model density minus spherical atom density with no anomalous dispersion corrections applied. Such maps were calculated from model structure factors for all measured intensities ($0.0 \leq \lambda^{-1} \sin\theta \leq 1.0$ Å^{-1}).

Theoretical Calculations.[29] The earliest attempts to understand the porphyrin ring came from calculations that modeled the π electrons as particles on a ring. This approach was improved and extended by Hückel calculations that led to a clearer understanding of the eigenvalue system. For the free base these calculations used the famous "four-orbital" pattern to explain the UV–visible spectra. The highest occupied levels were found to be nearly degenerate a_{2u} and a_{1u} π bonds, and the lowest unoccupied state was a symmetry-degenerate e_g π bond. Later semiempirical calculations extensively employed the Pariser–Parr–Pople and iterative extended Hückel formalisms.[30]

More recently, ab initio calculations have been carried out for the free base and metalloporphyrins. Optical transitions, photoelectron binding energies, and hyperfine fields have been calculated for Fe and Cu complexes of the closely related tetraazaporphyrin, as well as for the free base.[21] In these molecules nitrogen atoms are substituted for the C_m[31] atoms. Furthermore, calculations on Cu and Ag porphine have been performed both by the discrete variational method described below[32] and by the multiple-scattering Xα technique.[33] Floating spherical Gaussian calculations have also been performed.[34]

Because the discrete variational method (DVM) has been discussed thoroughly elsewhere,[35] only an outline of the technique is presented here. The method uses the Slater approximation for exchange,[36] in which the exchange portion of the total Hamiltonian is approximated by the form

$$V_{x\sigma} = -3\alpha\left[\frac{3\rho_\sigma}{4\pi}\right]^{1/3} \quad (1)$$

where ρ_σ is the charge density for σ (= ↑, ↓) spin electrons. The value of the scaling parameter, α, depends on which of several approximations is chosen but is in the range 0.667–1.0. In this work we have used a value of 0.70. An initial charge density $\rho_\sigma^{(0)}$ is formed by assuming a set of coefficients that weight a set of basis functions. Solution of the Schrödinger equation determines a new linear combination of basis

(13) Barry, C. D.; Hill, H. A. O.; Mann, B. E.; Sadler, P. J.; Williams, R. J. P. *J. Am. Chem. Soc.* **1973**, *95*, 4545–4551.
(14) Gouterman, M.; Stevenson, P. E. *J. Chem. Phys.* **1962**, *37*, 2266.
(15) Treibs, A. *Justus Liebigs. Ann. Chem.* **1929**, *476*, 1.
(16) Little, R. G.; Ibers, J. A. *J. Am. Chem. Soc.* **1974**, *96*, 4447–4452.
(17) Ulman, A.; Gallucci, J.; Fisher, D.; Ibers, J. A. *J. Am. Chem. Soc.*, **1980**, *102*, 6852–6854.
(18) Ulman, A.; Fisher, D.; Ibers, J. A. *J. Heterocycl. Chem.* **1982**, *19*, 409–413.
(19) Jameson, G. B.; Ibers, J. A. *Inorg. Chem.* **1979**, *18*, 1200–1208.
(20) Stevens, E. D. *J. Am. Chem. Soc.* **1981**, *103*, 5087–5095.
(21) Berkovitch-Yellin, Z.; Ellis, D. E. *J. Am. Chem. Soc.* **1981**, *103*, 6066–6073.
(22) Dunitz, J. D. "X-ray Analysis and the Structure of Organic Molecules"; Cornell University Press: Ithaca, NY, 1979; Chapter 8, pp 391–417.
(23) Stevens, E. D. "Mathematical Tools in Crystallography, ACA Tutorial"; American Crystallographic Association Winter Meeting, Eufaula, Alabama, 1980; pp 83–98.
(24) Wiest, R.; Rees, B.; Mitschler, A.; Mathey, F. *Inorg. Chem.* **1981**, *20*, 2966–2970.
(25) Cruickshank, D. W. J. *Acta Crystallogr.* **1949**, *2*, 65–82.
(26) Our full-matrix least-squares multipole refinement was carried out with a locally modified version of the program MOLLY81 by N. K. Hansen and P. Coppens.
(27) Hansen, N. K.; Coppens, P. *Acta Crystallogr., Sect. A* **1978**, *A34*, 909–921.
(28) All electron density maps were calculated with a locally modified version of NIELSAV (E. D. Stevens and N. K. Hansen), a program for the calculation of an exact three-dimensional Fourier summation in an oblique plane.
(29) For a general review of early porphyrin calculations, see: Chantrell, S. J.; McAuliffe, C. A.; Munn, R. W.; Pratt, C. A. *Coord. Chem. Rev.* **1975**, *16*, 259–284.
(30) (a) Roos, B.; Sundbom, M. *J. Mol. Spectrosc.* **1970**, *36*, 8–25. (b) Schaffer, A. M.; Gouterman, M. *Theor. Chem. Acta* **1972**, *25*, 62–82. (c) Basu, S. *Indian J. Phys.* **1954**, *28* 511–521. (d) Gouterman, M.; Wagniere, G. H.; Snyder, L. L. *J. Mol. Spectrosc.* **1963**, *11*, 108–127. (e) Henriksson, A.; Sundbom, M. *Theor. Chim. Acta* **1972**, *27*, 213–222. (f) Henriksson, A.; Roos, B.; Sundbom, M. *Ibid.* **1972**, *27*, 303–313. (g) Chen, I.; Abkowitz, M.; Sharp, J. H. *J. Chem. Phys.* **1969**, *50*, 2237–2244. (h) Chen, I. *J. Mol Spectrosc.* **1967**, *23*, 131–143.
(31) In the text C_a refers to the α-pyrrole carbon atoms, C_b refers to the β-pyrrole carbon atoms, and C_m refers to the meso carbon atoms. Hoard, J. L. *Ann. N.Y. Acad. Sci.* **1973**, *206*, 18–31.
(32) Ellis, D. E.; Berkovitch-Yellin, Z. *J. Chem. Phys.* **1981**, *74*, 2427–2435.
(33) Case, D. A.; Karplus, M. *J. Am. Chem. Soc.* **1977**, *99*, 6182–6194.
(34) Spangler, D. P. *Diss. Abstr.* **1979**, *39*(12, Pt 1) 5952.
(35) (a) Baerends, E. J.; Ellis, D. E.; Roos, B. *Chem. Phys.* **1973**, *2*, 41–51. (b) Rosen, A.; Ellis, D. E.; Adachi, H.; Averill, F. W. *J. Chem. Phys.* **1976**, *65*, 3629–3634.
(36) Slater, J. C. "Quantum Theory of Molecules and Solids"; McGraw-Hill; New York, 1974; Vol. 4.

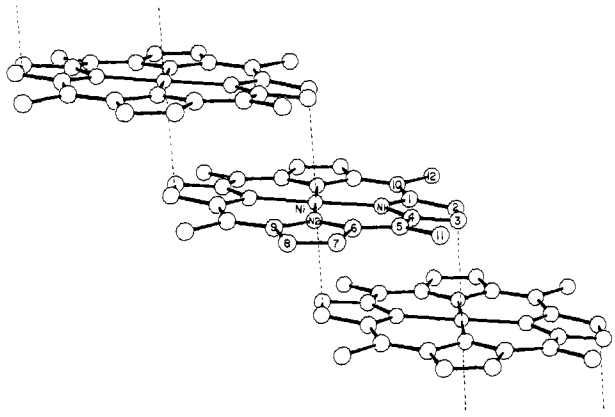

Figure 1. Illustration of the slipped-stack packing arrangement of three molecules of Ni(TMP) with hydrogen atoms omitted for clarity. The Ni atom of each molecule lies on a crystallographic inversion center. The distance from the midpoint of the C(2)–C(3) bond to the adjacent Ni atom is 3.297 Å.

functions and a set of eigenvalues that are then used to generate the next charge density, $\rho_\sigma^{(1)}$, etc. To facilitate the calculation of the Coulomb potential, the true charge density, which arises directly from the molecular orbitals, is approximated by a sum of charge densities centered on the atoms comprising the molecule. This is accomplished by a modified Mulliken population analysis of the basis set, in which the off-diagonal charge elements are apportioned to the contributing basis functions by a weighting factor that depends on the size of the corresponding diagonal elements.

While this "self-consistent-charge" (SCC) procedure lacks the rigor inherent in the use of the fully determined charge density, it has the advantage of being much faster to execute and affords a rather objective interpretation of the importance of the basis orbitals in the bonding scheme of the molecule. On an absolute basis these values may be errant; however, a comparison between calculations on closely related molecules will generally be valuable.

The Hamiltonian and overlap integrals were evaluated by using a Diophantine integration mesh of 1800 sampling points for Ni(P) and a minimal basis (Ni core + 3d,4s,4p; N core + 2s,2p; C core + 2s,2p; H 1s) calculation for Ni(TMP), and 3600 points for all extended basis (see below) calculations of Ni(TMP). The point set was generated from subsets of points centered on atomic centers so as to give a maximum point density in those regions wherein the integrand is most variable. For the Ni(TMP) and Ni(P) calculations the basis functions were derived numerically from the isolated, neutral atoms. A minimal basis set was employed for all atoms except nitrogen, the crucial factor in the binding of the metal to the ring. Thus for nitrogen, 3s and 3p functions, which were localized by solving the atomic problem within a potential well, were also added to the basis. (In some previous calculations, after an initial solution was obtained with a neutral atom basis, a second basis was defined, based on the self-consistent configuration found for the molecule, according to the SCC procedure. However, this basis offered little improvement probably owing to the inherent limitations of the populations analysis underlying the SCC scheme.) The 1s core orbitals of the carbon and nitrogen atoms and the 1s, 2s, 2p, 3s, and 3p orbitals of the nickel atom were kept "frozen" in a fully occupied configuration, and were thus excluded from the variational calculation. Valence states were constrained to remain orthogonal to the atomic cores. Initially, spin unrestricted calculations started with a single unpaired spin in the nickel d functions. The spin, however, quickly converged toward zero, so spin restricted calculations were employed thereafter. Thus Ni(TMP) is predicted to be diamagnetic.

The geometry for the tetramethyl derivative was idealized from preliminary crystallographic coordinates.[17] Although the molecule in reality has only an inversion center, the deviations from C_{4v} symmetry are small after rotation of two of the methyl groups. For the porphine calculations, the methyl groups were replaced by hydrogen atoms without altering the remainder of the skeleton. This replacement raises the symmetry to D_{4h}, but we again used the C_{4v} symmetry group in the calculations for ease of comparison with the tetramethyl compound.

The perturbed Ni(TMP) calculation was performed by allowing the charge distribution of two neighboring Ni(TMP) molecules to superimpose upon the molecular cluster under consideration. The perturbation is then reflected in the derived Coulomb and exchange potentials. These molecules were placed 3.3 Å on each side of the center molecule and were shifted along one axis such that the bond between the C_b atoms lay directly over the Ni atom. This model is almost identical with the crystal structure presented in Figure 1. The perturbing potential was updated on each SCF iteration, by assuming the electron density of the outer molecules to be identical with that being explicitly computed for the center molecule.

Table II. Crystallographic Bond Lengths (Å) and Angles (deg) for Ni(TMP)

	conventional refinement	high-order refinement	multipole refinement
Ni-N(1)	1.943 (1)	1.944 (2)	1.945 (1)
Ni-N(2)	1.963 (1)	1.966 (2)	1.966 (2)
N(1)-C(1)	1.385 (1)	1.385 (4)	1.384 (2)
N(1)-C(4)	1.383 (1)	1.377 (4)	1.377 (2)
N(2)-C(6)	1.387 (2)	1.385 (5)	1.382 (2)
N(2)-C(9)	1.381 (2)	1.374 (5)	1.378 (2)
C(1)-C(2)	1.437 (2)	1.436 (6)	1.430 (2)
C(3)-C(4)	1.442 (2)	1.446 (6)	1.441 (2)
C(6)-C(7)	1.435 (2)	1.439 (5)	1.432 (2)
C(8)-C(9)	1.440 (2)	1.440 (6)	1.438 (2)
C(2)-C(3)	1.331 (2)	1.356 (9)	1.348 (3)
C(7)-C(8)	1.337 (3)	1.349 (10)	1.356 (3)
C(1)-C(10)	1.378 (2)	1.380 (6)	1.382 (2)
C(9)-C(10)	1.378 (2)	1.387 (6)	1.386 (2)
C(4)-C(5)	1.375 (2)	1.373 (6)	1.378 (2)
C(5)-C(6)	1.380 (2)	1.392 (6)	1.394 (2)
C(5)-C(11)	1.517 (2)	1.513 (5)	1.506 (2)
C(10)-C(12)	1.516 (2)	1.511 (5)	1.511 (3)
N(1)-Ni-N(2)	89.98 (4)	90.0 (1)	89.93 (4)
N(1)-Ni-N(2)′	90.02 (4)	90.0 (1)	90.07 (4)
Ni-N(1)-C(1)	127.51 (8)	127.4 (2)	127.64 (8)
Ni-N(1)-C(4)	127.94 (9)	128.0 (2)	128.13 (9)
Ni-N(2)-C(6)	127.27 (9)	127.1 (2)	127.4 (1)
Ni-N(2)-C(9)	127.67 (9)	127.8 (3)	127.66 (9)
N(1)-C(1)-C(2)	110.5 (1)	111.2 (4)	111.2 (1)
N(1)-C(4)-C(3)	110.2 (4)	110.7 (4)	110.9 (1)
N(2)-C(6)-C(7)	110.1 (1)	110.6 (4)	110.9 (1)
N(2)-C(9)-C(8)	110.0 (1)	110.4 (4)	110.4 (1)
C(1)-N(1)-C(4)	104.5 (1)	104.6 (3)	104.2 (1)
C(6)-N(2)-C(9)	105.1 (1)	105.1 (2)	104.9 (1)
C(1)-C(2)-C(3)	107.3 (1)	106.5 (3)	106.8 (2)
C(4)-C(3)-C(2)	107.4 (1)	106.9 (3)	106.8 (1)
C(6)-C(7)-C(8)	107.4 (1)	106.5 (4)	106.6 (1)
C(9)-C(8)-C(7)	107.4 (1)	107.4 (4)	107.1 (1)
N(1)-C(1)-C(10)	126.6 (1)	126.8 (3)	126.5 (1)
N(1)-C(4)-C(5)	126.4 (1)	126.9 (3)	126.6 (1)
N(2)-C(6)-C(5)	126.2 (1)	126.4 (3)	126.1 (1)
N(2)-C(9)-C(10)′	126.0 (1)	126.1 (3)	126.1 (1)
C(4)-C(5)-C(6)	121.9 (1)	121.2 (3)	121.4 (1)
C(1)-C(10)-C(9)′	121.8 (1)	121.5 (3)	121.7 (2)
C(5)-C(4)-C(3)	123.4 (1)	122.3 (3)	122.5 (1)
C(5)-C(6)-C(7)	123.6 (1)	122.9 (4)	122.9 (1)
C(10)-C(1)-C(2)	122.9 (1)	121.9 (4)	122.3 (2)
C(10)′-C(9)-C(8)	123.9 (1)	123.5 (4)	123.4 (2)
C(4)-C(5)-C(11)	118.3 (1)	118.9 (5)	118.9 (2)
C(6)-C(5)-C(11)	119.8 (1)	119.8 (5)	119.6 (1)
C(1)-C(10)-C(12)	118.2 (1)	118.5 (5)	118.6 (1)
C(9)′-C(10)-C(12)	120.0 (1)	120.1 (5)	119.6 (1)

Results

Structural Features. As illustrated in Figure 1, Ni(TMP) is an essentially planar complex that forms one-dimensional slipped-stack chains in the crystal structure. The Ni atom lies on a crystallographic inversion center and thus only one-half of the molecule is unique. Chemically equivalent bond distances and angles in the porphyrinato macrocycle are equal within experimental error. One interesting and heretofore unexplained (vide infra) structural feature of this molecule is the significant difference between the two unique Ni–N bond lengths (Ni–N(1) = 1.943 (1) and Ni–N(2) = 1.963 (1) Å). We feel that this structural difference is real because it is also found after refinement of a less accurate data set collected from a different crystal.[17]

Table II is a comparison of the bond lengths and angles derived from the conventional, high-order, and multipole refinements. A comparison of these metrical parameters reveals the following: (i) the Ni–N bond length difference is not affected by the type

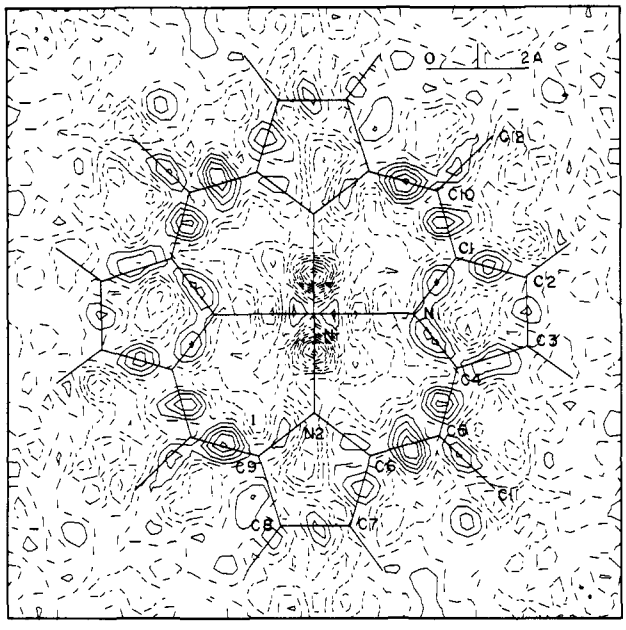

Figure 2. Difference electron density map calculated at the end of the conventional least-squares refinement through a plane defined by the Ni and N atoms. Contours are at 0.08 e Å^{-3} intervals with zero and negative contours dashed.

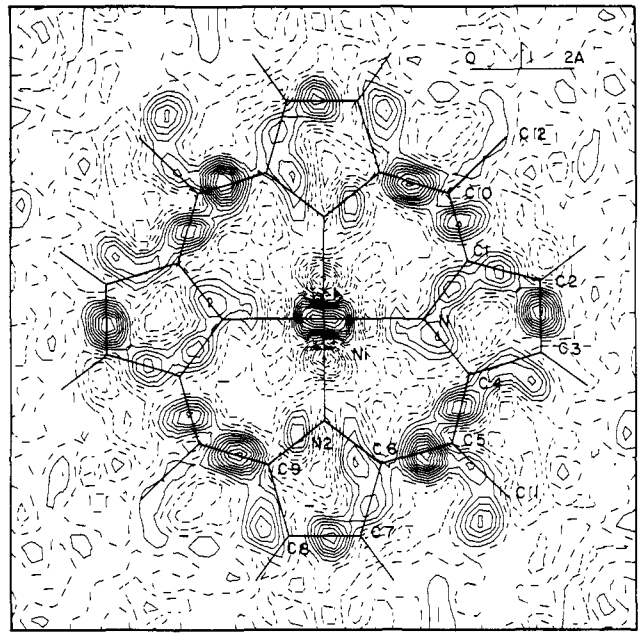

Figure 3. *Observed* deformation density ($X - X_{HO}$) plotted through a plane defined by the Ni and N atoms. Contours are as in Figure 2.

of refinement process; (ii) the largest bond length changes occur for the C_b–C_b bonds (C(2)–C(3) and C(7)–C(8)) where both high-order and multipole refinements lead to longer bonds relative to the conventional refinement; (iii) the C_a–C_m bonds associated with the N(1) pyrrole ring (C(1)–C(10) and C(4)–C(5)) are not affected by the method of refinement while the C_a–C_m bonds associated with the N(2) pyrrole ring (C(5)–C(6) and C(9)–C(10)) are lengthened by the high-order and multipole refinements.

A final difference electron density map ($F_o - F_c$) calculated through the plane of the porphyrin at the end of the conventional refinement is shown in Figure 2. There is positive density between all of the non-hydrogen atoms in the porphyrinato macrocycle although lone-pair density on the nitrogen atoms is not resolved. The difference density around the nickel atom has *mm* symmetry in the plane of the porphyrin rather than just the $\bar{1}$ symmetry required by the space group. There is also a lack of spurious charge buildup ("ghost peaks") near the metal atom, a problem that is often encountered in electron density studies involving metal-containing molecules.[37,38] These features indicate that the quality of the Ni(TMP) data set is sufficient for an electron density distribution study.

Bonding and lone-pair features are enhanced when difference electron density maps are calculated from parameters derived from high-order reflections (*observed* deformation maps). This is illustrated in Figure 3 where all of the positive density features have been intensified (although not all to the same degree) relative to the conventional difference electron density calculation. The largest peaks in the *observed* deformation map are associated with bonds that had the greatest lengthening after the high-order refinement: C(2)–C(3), 0.72 (11) e Å^{-3}; C(7)–C(8), 0.48 (11) e Å^{-3}; C(5)–C(6), 0.80 (11) e Å^{-3}; C(9)–C(10), 0.72 (11) e Å^{-3}. This is not surprising since atomic positions derived from a conventional refinement may be displaced toward regions of bonding or lone-pair density.[39] In the plane of the porphyrin, positive density is now found in the lone-pair region of atom N(1) while it is still unresolved for atom N(2). A negative region lies between each of the N atoms and the Ni atom.

Neighboring molecules of Ni(TMP) in the same stack (Figure 1) are oriented so that the C(2)–C(3) bond of one molecule is parallel and above the N(2)–Ni–Ni(2)′ atom sequence of its neighbor. The distance from the midpoint of the C(2)–C(3) bond to the adjacent Ni atom is 3.30 Å and the distance between symmetry related mean porphyrin planes is 3.35 Å.[40] This is comparable with the intrastack interplanar spacing (3.29 and 3.30 Å) between donor and acceptor molecules in the π molecular complex Ni(TMP)TCNQ[4] and falls within the range (3.2–3.5 Å) taken by Herbstein[41] to indicate donor–acceptor charge-transfer interaction. One consequence of this packing arrangement is that the square-planar Ni atom has a close intermolecular contact in each axial direction to achieve a pseudooctahedral environment. The coordination geometry around the Ni atom is similar to that found in the structures of the bis(toluene) solvates of Mn(TPP),[3,8] Zn(TPP),[9] and Cr(TPP).[10] In all three derivatives the porphyrin core is sandwiched between two toluene molecules with interplanar spacings in the range 3.30–3.37 Å. As Scheidt and co-workers have pointed out,[8-10] this particular coordination geometry implies π-complex formation, with the toluene molecules acting as π-donors and the metal atoms acting as π-acceptors. To extend this concept to Ni(TMP) implies that the molecule has hermaphroditic character, i.e., the Ni atom acts as a π-acceptor and the C_b–C_b bond (C(2)–C(3)) of the N(1) pyrrole ring acts as a π-donor. Indeed, as seen in Figure 3, there is a substantial charge buildup in the C(2)–C(3) bond relative to most of the porphyrin macrocycle, just as Stevens found for the C_b–C_b bond in Co(TPP).[20]

Figure 4a shows an *observed* deformation map calculated through a plane perpendicular to the plane of the porphyrin and including atoms N(1), Ni, and N(1)′. The large positive peaks above and below the Ni atom are cross sections of C_b–C_b (C(2)–C(3)) bonds from neighboring intrastack molecules. These C_b–C_b bonds are perpendicular to the N(1)–Ni–N(1)′ atom sequence. Figure 4b shows an *observed* deformation map calculated through a plane perpendicular to the plane of the porphyrin and including atoms N(2), Ni, and N(2)′. An explanation for the difference in Ni–N bond lengths (Ni–N(1) = 1.944 (2) and Ni–N(2) = 1.966 (2) Å) can be inferred from these two maps. A perturbation of the valence electron density of the Ni atom toward atoms N(1) and N(1)′ may result from the close proximity of the C_b–C_b bonds (Figure 4a). This possible back-bonding interaction could lead to a strengthening of the Ni–N(1) and Ni–N(1)′ bonds. In contrast the neighboring C_b–C_b bonds are

(37) Coppens, P. *Trans. Am. Crystallogr. Assoc.* **1980**, *16*, 39–77.
(38) Troup, J. M.; Extine, M. W.; Ziolo, R. F. In "Electron Distributions and the Chemical Bond"; Coppens, P., Hall, M., Eds.; Plenum Press: New York, 1982.
(39) Coppens, P. *Acta Crystallogr., Sect. B* **1974**, *B30*, 225–261.
(40) The midpoint of the C(2)–C(3) bond and the distances between planes were calculated by using parameters derived from the conventional refinement.
(41) Herbstein, F. H. *Perspect. Struct. Chem.* **1974**, *4*, 166–395.

Table III. Multipole Populations and Radial Exponents[a,b]

	Ni	N(1)	N(2)	C(1)	C(2)	C(5)	C(11)
κ	1.0	1.04 (1)	1.00 (1)	1.00 (2)	0.94 (1)	0.98 (2)	0.98 (2)
$\kappa'\zeta$	8.358 (8)	1.88 (2)	3.8 (2)	2.83 (5)	3.17 (3)	3.06 (5)	2.64 (3)
P_v	0.0	4.6 (1)	4.8 (1)	3.7 (2)	4.59 (7)	4.0 (2)	4.4 (1)
P_{00}	3.56 (6)	0.0	0.0	0.0	0.0	0.0	0.0
P_{11+}	0.0	0.0	0.0	0.04 (4)	0.03 (3)	−0.04 (4)	0.0
P_{11-}	0.0	0.0	0.0	0.02 (4)	−0.09 (3)	−0.14 (2)	0.0
P_{10}	0.0	0.48 (6)	0.13 (3)	0.0	0.0	0.0	−0.12 (6)
P_{20}	0.23 (3)	0.21 (6)	0.00 (3)	−0.22 (3)	−0.30 (3)	−0.17 (4)	−0.01 (5)
P_{22-}	0.08 (3)	−0.05 (6)	−0.14 (5)	0.11 (3)	−0.01 (3)	−0.14 (4)	0.0
P_{22+}	0.0	0.0	0.0	−0.21 (3)	−0.11 (3)	0.09 (2)	0.0
P_{30}	0.0	0.40 (7)	0.05 (2)	0.0	0.0	0.0	0.39 (5)
P_{31+}	0.0	0.0	0.0	−0.03 (2)	−0.08 (3)	−0.02 (3)	0.0
P_{31-}	0.0	0.0	0.0	−0.02 (3)	−0.01 (2)	0.06 (2)	0.0
P_{32+}	0.0	0.58 (8)	0.09 (3)	0.0	0.0	0.0	0.0
P_{33+}	0.0	0.0	0.0	0.29 (4)	0.29 (3)	0.35 (6)	0.35 (4)
P_{33-}	0.0	0.0	0.0	−0.07 (4)	0.20 (4)	−0.00 (2)	−0.15 (4)
P_{40}	−0.09 (2)	0.24 (9)	−0.02 (3)	0.06 (3)	0.02 (3)	−0.05 (4)	0.24 (6)
P_{42+}	0.14 (2)	0.34 (8)	−0.01 (4)	0.08 (3)	0.08 (3)	0.01 (4)	0.0
P_{42-}	0.0	0.0	0.0	0.12 (3)	0.03 (3)	0.08 (3)	0.0
P_{43+}	0.0	0.0	0.0	0.0	0.0	0.0	−0.14 (4)
P_{43-}	0.0	0.0	0.0	0.0	0.0	0.0	−0.31 (5)
P_{44+}	−0.29 (2)	0.20 (7)	0.07 (3)	0.16 (4)	0.19 (4)	−0.07 (5)	0.0
P_{44-}	0.0	0.0	0.0	0.08 (4)	0.01 (4)	−0.01 (3)	0.0

[a] ζ in au^{-1}, populations in e. [b] Values without standard deviations were not refined because of symmetry restrictions.

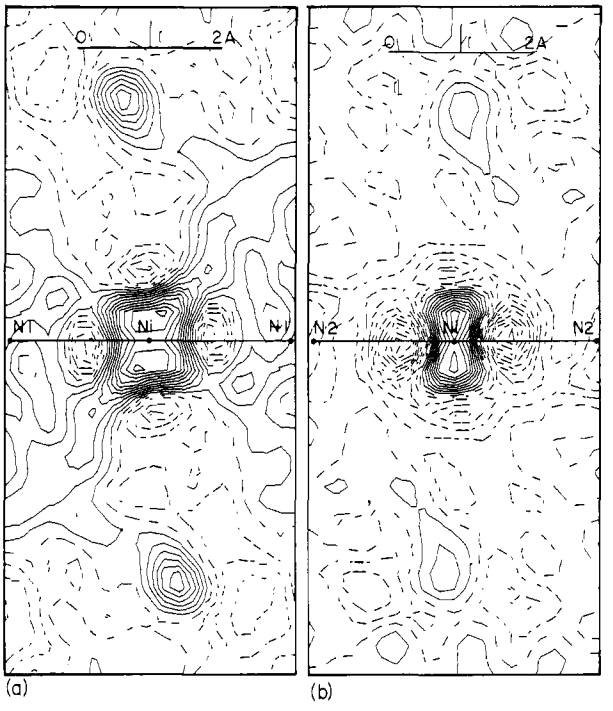

Figure 4. *Observed* deformation density ($X - X_{HO}$) (a) plotted through a plane that is perpendicular to the plane of the porphyrin that includes atoms N(1), Ni, and N(1)′; (b) plotted through a plane perpendicular to the plane of the porphyrin that includes atoms N(2), Ni, and N(2)′. Contours are as in Figure 2.

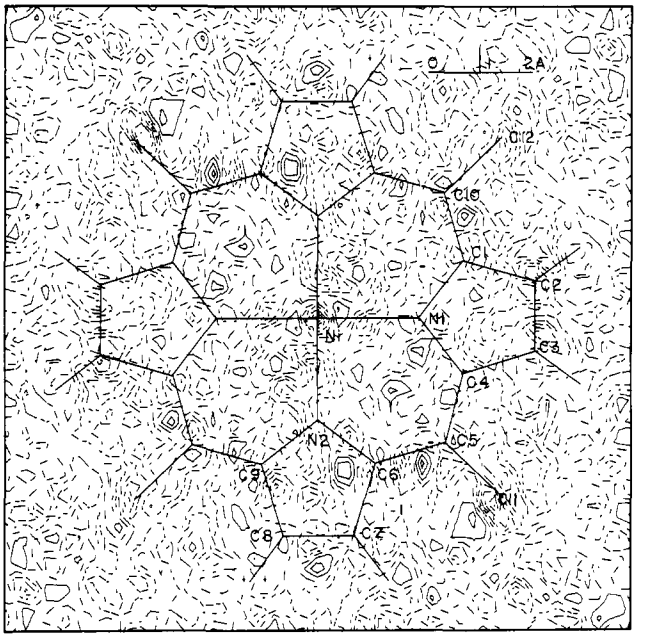

Figure 5. *Residual* density map (observed density minus aspherical model density) plotted through a plane defined by the Ni and N atoms. Contours are as in Figure 2.

parallel to the N(2)–Ni–N(2)′ atom sequence and as illustrated in Figure 4b there is no perturbation of electron density from the Ni atom toward atoms N(2) and N(2)′.

The inclusion of deformation functions (multipole model[27]) in the least-squares refinement allows one to model the aspherical valence electron density in a molecule. The derived multipole populations and radial exponents from the multipole refinement are listed in Table III. A *residual*[20,23] density map (observed density minus aspherical model density) calculated at the end of a multipole refinement should be featureless if the aspherical density has been well modeled. A map of this type for Ni(TMP) is shown in Figure 5. There are no large discrepancies between the observed and multipole densities. However there are several small positive peaks near bond midpoints that are probably due to the inherent inadequacy of atom deformation constraints (Table I, footnote *c*). A *model*[20,23] deformation map (aspherical model density minus spherical model density) calculated through the plane of the porphyrin is displayed in Figure 6. Relative to the *observed* deformation map (Figure 3) several density features are now better resolved. In both maps there are negative regions between the Ni atom and the N atom of the pyrrole rings. However, in the *model* deformation map the density around the Ni atom in the plane of the porphyrin is resolved into four positive peaks that are directed away from the nitrogen atoms and toward the methine carbon atoms. The nitrogen lone-pair densities are also well resolved, and there is evidence from both the *model* and *observed* deformation maps that there is more of a charge density concentration in the N(1) lone pair compared with N(2). Despite the deformation constraints applied to chemically equivalent atoms, all of the corresponding bond peak heights agree within one contour level between the *model* and *observed* maps. Figure 7a,b shows *model* deformation maps perpendicular to the plane of the

Table IV. Mulliken Population Analysis

potential type	orbital	Ni(P) (extended basis)	Ni(TMP) (minimum basis)	Ni(TMP)[a] (unperturbed) (extended basis)	Ni(TMP)[a] (perturbed) (extended basis)
Ni	3d	8.71	8.76	8.76	8.66
	4s	0.19	0.23	0.31	0.31
	4p	0.23	0.19	0.39	0.37
	charge	+0.88	+0.82	+0.63	+0.66
N	2s	1.42	1.56	1.36, 1.36	1.36, 1.36
	2p	3.60	3.76	3.57, 3.54	3.56, 3.53
	3s	0.07		0.09, 0.09	0.09, 0.09
	3p	0.12		0.13, 0.15	0.13, 0.15
	charge	−0.21	−0.32	−0.15, −0.14	−0.14, −0.12
C_a	2s	1.12	0.98	1.16, 1.12	1.16, 1.11
	2p	2.78	2.92	2.86, 2.87	2.86, 2.90
	charge	+0.10	+0.10	−0.03, +0.01	−0.02, −0.01
C_b	2s	1.20	1.18	1.18, 1.25	1.18, 1.24
	2p	3.14	3.15	3.09, 3.15	3.09, 3.16
	charge	−0.33	−0.33	−0.27, −0.40	−0.27, −0.41
C_m	2s	1.15	1.07	0.99	0.99
	2p	3.29	2.98	2.97	2.96
	charge	−0.44	−0.05	+0.04	0.05
C_{methyl}	2s		1.38	1.41	1.40
	2p		3.63	3.55	3.53
	charge		−1.01	−0.97	−0.92
$H_{equatorial}$[b]	1s		0.69	0.69, 0.67	0.72, 0.67
	charge		+0.31	+0.31, +0.33	+0.28, +0.33
H_{axial}[b]	1s		0.57	0.64	0.67
	charge		+0.43	+0.36	+0.33
H_b(TMP)	1s		0.71	0.76, 0.63	0.76, 0.64
	charge		+0.29	+0.24, +0.37	+0.23, +0.36
H_m(P)	1s	0.69			
	charge	+0.31			
H_b(P)	1s	0.71			
	charge	+0.29			

[a] C_{2v} symmetry was assumed. For atoms that have two sets of values, those on the left are for atoms lying closer to the x axis, and those on the right are for atoms lying closer to the y axis. [b] The two methyl hydrogen atoms lying closest to the porphyrin plane are labeled "equatorial" and the more distant hydrogen atom is labeled "axial".

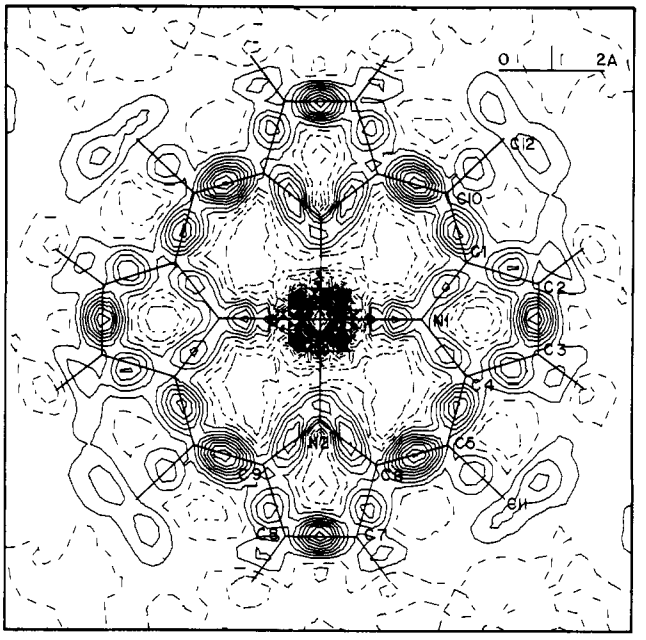

Figure 6. *Model* deformation density (aspherical model density minus spherical model density) plotted through a plane defined by the Ni and N atom positions. Contours are as in Figure 2.

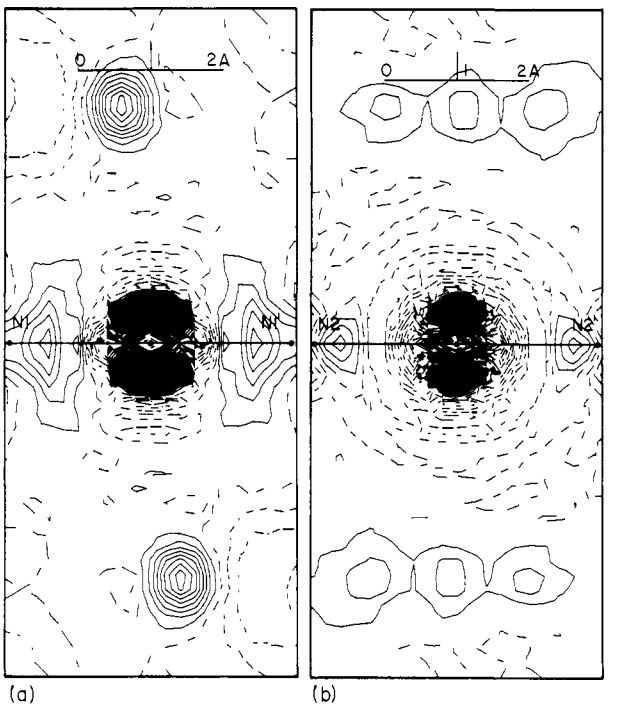

Figure 7. *Model* deformation density (aspherical model density minus spherical model density) (a) plotted through a plane that is perpendicular to the plane of the porphyrin which includes atoms N(1), Ni, and N(1)′; (b) plotted through a plane perpendicular to the plane of the porphyrin that includes atoms N(2), Ni, and N(2)′. Contours are as in Figure 2.

porphyrin. These maps are defined by the same atoms as the *observed* deformation maps in Figures 4a and 4b and contain features that are qualitatively similar. Note that the elongation of charge density perpendicular to the Ni–N(1) bond (Figure 4a, *observed* deformation density) is reproduced by the multipole model (Figure 7a).

Comparison of Molecular Calculations of Unperturbed Ni(TMP) and Ni(P). (a) Population Analysis, Energy Levels, and Density of States. While again it must be cautioned that the Mulliken population analysis is an artificial device for assigning charge to atoms, a comparison between similar molecules is enlightening. These populations for Ni(TMP) and Ni(P) with extended bases

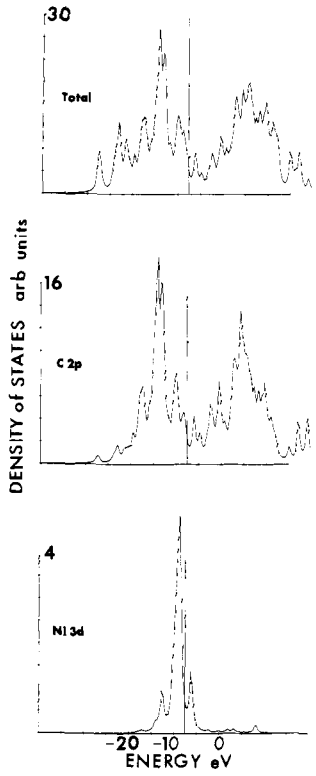

Figure 8. Total and partial densities of states for the extended basis calculation of Ni(TMP), broadened by a Lorentzian function of 0.4 eV. The top panel is the total density of states, the middle is the partial density of states for C 2p orbitals, and the bottom is the partial density for Ni 3d functions. The vertical line marks the Fermi energy.

are given in columns 1 and 3 of Table IV and one immediately sees that the Ni, N, C_a, and C_b charges and populations are similar for the two molecules. The slight increase in electron density on the Ni atom goes primarily into the Ni 4p orbitals, as the d orbital population remains almost exactly the same. The 2s orbitals of all the carbon atoms show extensive hybridization with the 2p levels, and the hydrogen sites in all cases show a sizable positive charge. (Note that calculations on the Ni(TMP) were also done with a minimal basis, that is without the inclusion of 3s and 3p states on N. This calculation agreed fairly well with the extended basis case as shown by the Mulliken populations in column 2 of Table IV. The most significant difference, as should be expected, occurred in the N populations. Inclusion of the 3s and 3p states raises the charge from −0.32 to −0.15.)

The largest difference between Ni(TMP) and Ni(P) is the charge density on the C_m atom, where the presence of the methyl group greatly decreases the negative charge on this bridging carbon nucleus (from −0.44 in the porphine to essentially zero in TMP). The methyl carbon atom itself bears a large negative charge, but the methyl group as a whole is essentially neutral. Hence, the methyl group draws electrons from the C_m atom, causing only a very slight change in negative charge density in most of the other atoms in the molecule with the exception of the C_m atoms.

Partial and total density of states plots provide another useful way of viewing the results. The contribution to a molecular orbital from any basis state is given by its Mulliken population. The partial density of states function for atomic basis function j is given by[32]

$$D_j(E) = \sum_n f_{nj}(\pi/\Gamma)/((E - E_n)^2 + \Gamma^2) \qquad (2)$$

which includes a Lorenztian broadening factor Γ (0.4 eV was used in this case). Here f_{nj} is the Mulliken weight of basis orbital j in molecular eigenvector n. Total and partial densities of states for Ni(TMP) are shown in Figure 8. (Analogous plots for Ni(P) are qualitatively similar.) The largest peak, comprising mostly carbon and nitrogen 2p orbitals, is centered around −14 eV and is substantially larger in the TMP calculation relative to the other maxima. This is the result of the addition of methyl carbon p orbitals which are sharply peaked in energy, reflecting the inability of these carbon atoms to interact strongly with the conjugation. The partial density of states of the Ni 3d orbital is very similar in the two cases. The d_{z^2} component is fairly tightly localized in the $10a_1$ level of Ni porphine, and the $12a_1$ level of TMP, both contributing 87% to the composition of the molecular orbitals. The d_{xy} function has the proper symmetry for in-plane π bonding, but this is not used to any large degree, and the $7b_2$ and $9b_2$ states of porphine and TMP, respectively, are almost totally composed of nickel d character. Considerable π interaction does, however, occur in e symmetry (d_{xz}, d_{yz}). The metal d charge is distributed in the porphine to the 13e (30%), 14e (18%), and 15e (47%) states, and in the TMP into the 16e (18%), 17e (24%), and 18e (51%) orbitals.

An interesting contrast between the TMP and the porphine occurs in the σ bonding b_1 symmetry. In the porphine calculation, the $d_{x^2-y^2}$ charge is mostly distributed to the $6b_1$ (30%) and the $9b_1$ (54%) levels. In TMP, on the other hand, a near degeneracy occurs between the $7b_1$ and $8b_1$ states, and the d density is partitioned among the $7b_1$ (19%), $8b_1$ (16%), and the $10b_1$ (53%) states. In both cases the highest of these b_1 states is the lowest unoccupied orbital, and is apparently high enough to encourage spin pairing, yielding a diamagnetic molecule. The crystal field splittings are similar for these two molecules, and are roughly the same as those found for Cu porphine in a previous calculation.[32] The perpendicular crystal field splitting, b_{1g}–e_g, is 2.2 and 2.4 eV for porphine and TMP, respectively, and the parallel value, b_{1g}–b_{2g}, is 3.0 eV in both cases. The latter value is the same as for the parallel splitting of copper porphine. Note that the pattern of the splitting, with the d_{xz} and d_{yz} levels occurring above the d_{xy}, is in variance with standard crystal field theory, presumably because of the extensive π interaction.

Another contrast between Ni(TMP) and Ni(P) is the order of the two highest occupied levels. In both systems the highest occupied a_1 state (a_{2u} in D_{4h} nomenclature) is primarily formed from the nitrogen and C_m p_z orbitals, and the highest occupied a_2 state (a_{1u} in D_{4h} symmetry) is composed of the p_z levels on the C_a and C_b atoms. In the porphine the $5a_2$ ($11a_u$) state lies very slightly above the $11a_1$ ($3a_2$ state), though by only a few hundredths of an eV, which is well within the errors of the computational approximations. In the TMP calculations, however, the $13a_1$ state is higher than the $6a_2$ by about 0.25 eV, which probably is significant.

(b) Total Valence Density. Plots of the true charge density, i.e., the charge density calculated directly from the eigenfunctions, rather than projected through the Mulliken scheme, confirm the observations of the previous section. The in-plane densities from valence orbitals are essentially identical for TMP and porphine except for the region of C_m atoms, where, as mentioned above, there is considerably greater electron density in TMP. There also appears to be very slightly more charge located between C_a and C_b atoms, but this may be artifactual.

A better view of the bonding regions of the molecule is obtained from plots of the difference of the total, true density, and the projected Mulliken density. Deviations from zero reveal perturbations the molecular environment imposes on the isotropic atomic functions. Again the plots show the similarity between the TMP and the porphine compound in the central portion of the molecule, and the increased density around the C_m atom of TMP, which leads to more bonding interaction between the C_a and C_m carbon atoms.

Comparison between Perturbed and Unperturbed Ni(TMP). The motivation for studying a molecule of Ni(TMP) under the influence of fields of nearest neighbors was to seek an explanation for the observed 0.020 (1)-Å difference between the two sets of Ni–N bond lengths. For the purposes of the following discussion, the reference system will be defined such that the position of the neighboring Ni(TMP) molecules was obtained by translating along the x and z axes. With this definition the solution to the trimer problem would require the mixing of basis functions centered on each of the 147 atoms composing the trimer—a calculation which

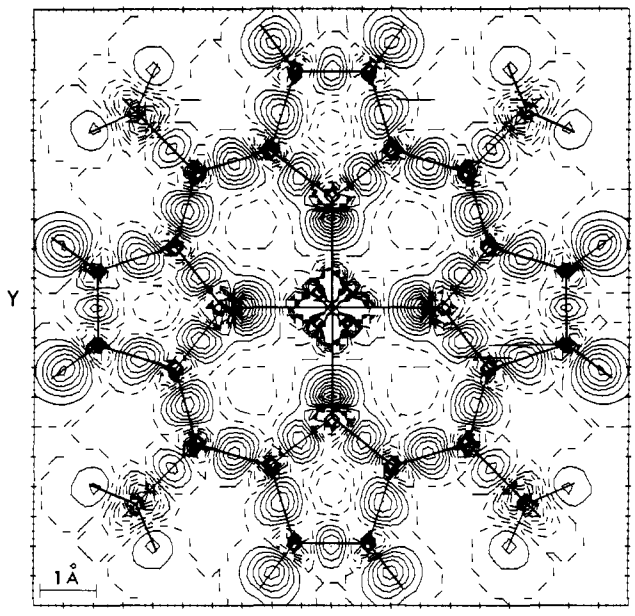

Figure 9. Theoretical contour plot of the xy plane of Ni(TMP). The difference density is plotted, defined as the full valence density minus Mulliken optimized spherical densities. Contours are spaced at 0.08 e/Å^3 intervals, and dotted lines show negative contours. The horizontal Ni–N bonds are the shorter ones experimentally.

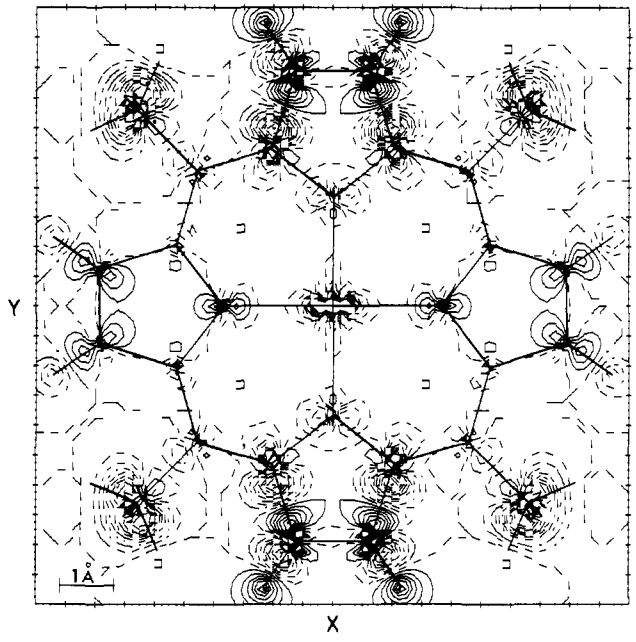

Figure 10. Theoretical contour plot of the charge density difference between Ni(TMP) perturbed by two neighbors, and unperturbed Ni(TMP). Contours are plotted at intervals of 0.002 e/Å^3, and dotted lines indicate negative values. The horizontal Ni–N bonds are the shorter ones experimentally.

is currently too ambitious. A simpler approximation is to solve for eigenlevels associated only with the center molecule, but adding the charge density from the outer molecules in the evaluation of the Hamiltonian matrix elements. Addition of the perturbation lowers the symmetry from C_{4v} to C_{2h} (assuming that appropriate rotation of methyl groups to obtain maximum symmetry will not significantly alter the Ni–N region). Since integral evaluations based on a finite sample of integration points will invariably bias charge densities, two coupled calculations were done to minimize this effect. In one calculation the unperturbed Ni(TMP) was solved in C_{2h} symmetry. Then, with an identical integration point mesh, the perturbed system was solved. In this way a comparison between perturbed and unperturbed species is nearly independent of the idiosyncrasies of the set of sample points.

As can be seen in Table IV the Mulliken values are affected to only a very minor extent by the perturbation. Though the Fermi energy of the perturbed system is about 0.5 eV higher than the unperturbed system, after correction for this offset the eigenvalues are for the most part very nearly the same. The exceptions to this are, unsurprisingly, those orbitals composed primarily of p_z orbitals of ring atoms. For these states the perturbation is sufficient to alter energies by between 0.3 and 0.5 eV for a few states.

Again in order to minimize the integration set bias, the charge density map shown in Figure 9 has been prepared by averaging charge densities at points that for the unperturbed system would be equivalent had the calculation employed the full C_{4v} symmetry. The small alterations induced by the perturbation were added to this averaged charge density to complete the map.

A point by point comparison of the charge density of the perturbed molecule minus that of the unperturbed molecule yields a map for the xy plane shown in Figure 10. (Since we were concerned with the intramolecular response to the perturbation, only the charge density from the center molecule is plotted. The small amount of charge density leaking from the neighbors is not included.) A positive value indicates that the perturbation increased the electron density, and a negative value means that the electron density was diminished. Of particular interest is that for all Ni–N bonds the perturbation seems to enhance the charge separation along the Ni–N axes, showing a negative region nearer the Ni site and a positive region nearer the N site. That this effect is larger for the shorter Ni–N bonds (x axis in Figures 9–11) seems reasonable since the perturbing molecules are allowed by symmetry to have a dipole moment across the pyrrole ring in this direction, whereas such a moment is forbidden in the perpendicular direction. It is clear that this effect has slightly enhanced the electrostatic attraction of the Ni and x-axis nitrogen atoms, thus tending to shorten the bond. Consideration of only the length of the Ni–N bond is probably too simplistic, however, since this distance is also influenced by the interaction between the N and the C_a atoms. These perturbation calculations were carried out with an idealized square-planar Ni environment, and it is apparent that the perturbation alone is insufficient to induce the charge density differences along the x and y axes that are observed experimentally.

Other perturbation effects are the differences in the two pyrrole rings. The ring along the x axis that resides in the region of the perturbing molecule between the Ni and N atoms has received charge density. On the other hand, the pyrrole ring along the y axis is near the methyl group hydrogen atoms and is far more severely influenced, with a reasonably large polarization of the C_a–C_b bond. This, however, does not necessarily have a physical meaning, since the methyl groups have been rotated to maximize the symmetry.

In order to gauge the magnitude of the perturbation-induced electron density rearrangements, we tried a similar calculation in which one set of N atoms was placed 0.01 Å nearer the Ni nucleus than in the square-planar arrangement, and the other set was displaced 0.01 Å farther from the Ni. This distortion exhibited two effects, which are shown in Figure 11, a plot of the difference in charge density between a distorted (C_{2v}) geometry and an undistorted geometry. Note that the contour intervals are 5 times those for the analogous perturbation contour plot (Figure 10). For the shortened bond (x axis), electron density was displaced from the Ni end of the bond to the N end, whereas for the lengthened bond (y axis), the charge movement was in the opposite direction. Hence, it appears we are in a range of nuclear separations in which decreasing distance enhances the electron transfer inherent in ionic bonding. Furthermore, the distortions in the charge density are several times larger than those observed in the perturbation calculation. Thus, while the perturbation of the molecule by intrachain packing appears to be insufficient to generate the observed charge density differences along the two sets of Ni–N bonds, a geometrical distortion is able realistically to portray this difference. Consequently, though the calculations are able in some degree to mimic these differences, one cannot conclude that the 0.02-Å difference is necessarily due to the

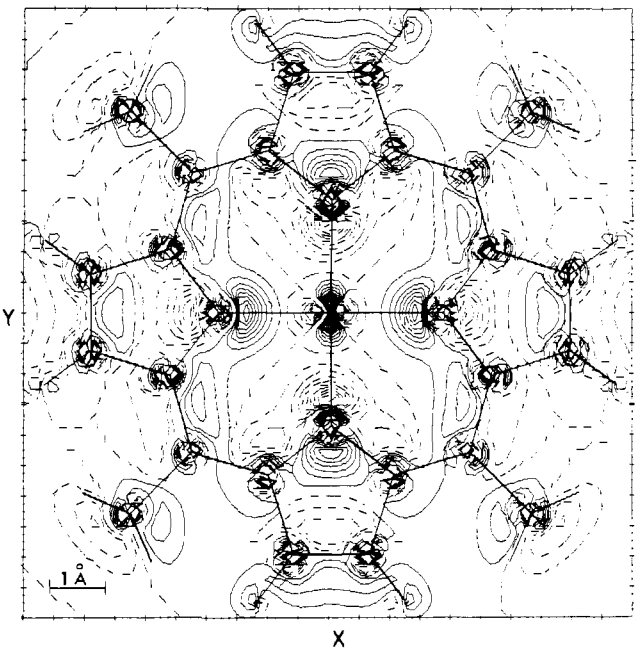

Figure 11. Theoretical contour plot of the charge density difference caused by shortening the horizontal Ni–N bond and lengthening the vertical Ni–N bond to give a 0.02-Å difference. Contours are plotted at intervals of 0.01 e/Å^3, and dotted lines indicate negative values.

perturbation. However, we speculate that small motions initiated by the perturbation might precipitate further charge density alterations that continue the nuclear rearrangement. This suggests the necessity of a full geometric optimization, a set of calculations that is unfortunately untenable.

Finally, contour density maps of the π planes (planes perpendicular to the Ni–N framework) exhibit a lowering of the charge near the *xy* plane and a rise about 1 Å away from the plane. It is tempting to imagine this to be a manifestation of incipient intermolecular bonding. However, care must be exercised, since the Mulliken approximation to the potential is rather crude, and it is difficult to eliminate the possibility of computational artifacts at this level.

Comparison of Experimental and Theoretical Results. The experimental deformation maps (Figures 3–7) are composed of thermally smeared densities while the theoretical deformation maps (Figures 9–11) are composed of static densities. Because of this basic difference in models comparisons will be kept at a qualitative level.

In the vicinity of the Ni atom the difference density is remarkably similar for both the multipole *model* map (Figure 6) and the *theoretical* perturbed model map (Figure 9). One sees negative regions between the N lone-pair regions and the Ni atom as well as four positive peaks near the Ni atom pointing toward the C_m atoms. In addition, the inequality of the N lone-pair charge densities is consistent between the maps, although the agreement is somewhat masked by the differences in the manner in which the experimental and theoretical difference maps are presented. In the experimental difference maps we have subtracted out neutral unperturbed atoms, while in the theoretical difference maps we have subtracted optimized ions based on Mulliken population analysis. Thus, the two-symmetry-inequivalent N atoms are represented as slightly different spherical ions, which reduces the difference between the two axes in the difference contours of Figure 9. However, this difference is observed in the total density plots. For instance, the charge difference between points about 1.5 Å from the Ni atom on the two axes is experimentally in the range of 0.1–0.2 e/Å^3, whereas the calculated difference in total charge density at this point is about 0.19 e/Å^3.

Within the porphyrinato macrocycle the comparisons are not as good. In the N(1) pyrrole ring the *model* deformation map shows a C_b–C_b bond with twice the charge density as the N–C_a and C_a–C_b bonds. The corresponding ring in the *theoretical* deformation map shows approximately equal charge density in all of the ring bonds. The inequality of charge densities for the C_a–C_m bonds in the *observed* and *model* deformation maps is not reproduced in the theoretical map. In general, the theoretical map shows more symmetry than the experimental map.

It is possible that the largest experimental–theoretical discrepancy, the amount of charge between the C_b atoms compared with that between other members of the ring, is related to the problem of adequately describing the C–H bonding. In this respect, it is interesting that while the calculated charge density is too small between the C_b atoms, it is too large between these carbon atoms and the ring hydrogen atoms, indicating that the bonding capacity of carbon is being channeled toward the hydrogen to too great a degree, according to the experimental results. This may be a result of the particular basis orbitals used, although the size of the disparity suggests this is at best only part of the answer. Higher order multipole contributions to the molecular potential may have to be included in order to reproduce such features.

Conclusion

Although concrete conclusions concerning the effect of packing forces on the electronic structure of an individual molecule are not forthcoming, at this point we feel the approach we have taken here is an encouraging initial attempt. While the calculations seem to indicate that the perturbation is by itself too small to engender the geometrical distortion from ideal symmetry found in Ni(TMP), the experimental electron densities do agree fairly well with those calculated with a geometrically distorted Ni environment. Furthermore, to understand completely how the intermolecular stack interactions affect the intramolecular geometry, one would probably have to obtain a geometrically optimized Ni(TMP) polymeric structure.

This combined theoretical and experimental study of the charge density of Ni(TMP) provides two independent descriptions of the valence electron density distribution. The fact that both descriptions agree well is encouraging, especially since both theory and experiment are pushed to the limit to obtain such descriptions. The usefulness of such a combined effort in characterizing structural features of interesting molecules seems clear.

Acknowledgment. This work was supported in part by the National Science Foundation through the Materials Research Center of Northwestern University (Grant DMR79-23573) and by the National Institutes of Health (Grant HL-13157 to JAI). We are indebted to Prof. P. Coppens for supplying several computer programs used in the analysis of the X-ray data.

Registry No. Ni(TMP), 67067-51-0; Ni(P), 15200-33-6; Ni, 7440-02-0; nitrogen, 7727-37-9.